

Photoinduced Energy and Electron Transfer Processes in Hexapyropheophorbide *a*-Fullerene [C₆₀] Molecular Systems

Martin Regehly,[†] Eugeny A. Ermilov,[†] Matthias Helmreich,[‡] Andreas Hirsch,[‡] Norbert Jux,^{*,‡} and Beate Röder^{*,†}

Institut für Physik, Photobiophysik, Humboldt Universität, Newtonstr. 15, D-12489 Berlin, Germany; Institut für Organische Chemie, Universität Erlangen-Nürnberg, Henkestr. 42, D-91054 Erlangen, Germany

Received: August 30, 2006; In Final Form: November 8, 2006

The photophysical properties of the novel hexapyropheophorbide *a* (**P6**), and hexakis (pyropheophorbide *a*)-C₆₀ (**FP6**) were studied and compared with those of hexakis (pyropheophorbide *a*)-fullerene [5:1] hexaadduct (**FHP6**). It was found that after light absorption the pyropheophorbide *a* molecules in all three compounds undergo very efficient energy transfer as well as partly excitonic interactions. The last process results in the formation of energy traps, which could be resolved experimentally. For **P6**, due to shorter distances between neighboring dye molecules, stronger interactions between pyropheophorbide *a* units than for **FHP6** were observed. As a consequence, the excitation energy is delivered rapidly to traps formed by stacked pyropheophorbide *a* molecules resulting in the reduction of fluorescence, intersystem crossing, and singlet oxygen quantum yields compared to the values of **FHP6**. For **FP6** the reduction of these values is much stronger due to an additional fast and efficient deactivation process, namely photoinduced electron transfer from pyropheophorbide *a* to the fullerene moiety. Consequently, **FP6** can be considered as a combination of a light-harvesting system consisting of several separate pyropheophorbide *a* molecules and a charge-separating center.

1. Introduction

The development of artificial donor–acceptor models mimicking the energy conversion in photosynthesis has been one of the important goals during the past two decades.^{1–8}

Among the large number of electron-transfer assemblies characterized, C₆₀-fullerene based systems have demonstrated great potential as photosynthetic reaction centers due to the capability of C₆₀ to act as an excellent electron acceptor.^{9–11} It has been shown also that C₆₀ can be used as a versatile building block for the construction of globular dendrimers.^{12,13} Dendrimers are highly branched molecules, with many end groups emanating from one central core. They can contain selected functional groups in predetermined sites of their tree-like structure and also host molecules in inner cavities and deep ditches caused by their multi-branched structure. Moreover, a large number of dye chromophores could be covalently coupled to a functional core of dendritic molecules. This design does not only allow the construction of light harvesting antenna systems,¹⁴ but has also been proven to be of superior significance for the development of drug delivery systems in medicine. In this context the modular carrier concept for photodynamic therapy of tumors is especially valuable.^{15–17}

Recently, we reported on the synthesis and photophysical properties of novel fullerene C₆₀-pyropheophorbide *a* (pyropheo) molecular systems.^{4–8,13} It was shown that in monofullerene–bispyropheo (**FP1**) the fullerene strongly affects the photoactivity of the pyropheo moieties due to the high electron accepting capabilities mentioned above. As a result, a strong reduction of

the fluorescence and the singlet oxygen quantum yields was observed for **FP1** compared to the values obtained for the reference compound bispyropheo (**P2**).⁴ If the conjugation of the π -electron system of the fullerene is broken up by the addition of five diethyl malonate addends in the remaining octahedral positions (monofullerene hexaadduct-bispyropheo: **FHP1**), the electron accepting ability of C₆₀ is strongly reduced and no photoinduced electron transfer occurs. For this reason **FHP1** can be treated as a first step on the way to a fullerene-based multiplying system in modular carriers for drug delivery.⁵

The next step on this way was to increase the number of added pyropheo molecules, and the compound hexakis(pyropheophorbide *a*)-fullerene[5:1] hexaadduct (**FHP6**) had been synthesized. It was found that in **FHP6** the fluorescence as well as singlet oxygen quantum yields were quenched compared to those values of the reference **FHP1**. These results were explained by applying the phenomenological model of energy traps and efficient delivery of excitation to them via Förster energy transfer.⁸

The highest number of pyropheo molecules linked to a fullerene was realized in the synthesis of a C₆₀-hexaadduct carrying 12 dye molecules (**FHP12**).⁶ Spectroscopic investigations of this compound in comparison with **FHP1** and **FHP6** revealed that formation of energy traps is more probable for **FHP12** compared to systems with lower number of pyropheo molecules. The reason for this observation is a higher local concentration of dye molecules and the resulting shorter distances between them. As a consequence, the photoexcited dye molecules are mainly deactivated by intramolecular nonradiative decay processes. All these observations together clearly demonstrate the importance of the fullerene core as well as the conformation of the covalently bound dendritic dye system for the relative efficiency of different deactivation processes after photoexcitation.

* Corresponding author phone: +49 30 2093 7625; fax: +49 30 2093 7666; e-mail: roeder@physik.hu-berlin.de.

[†] Humboldt Universität.

[‡] Universität Erlangen-Nürnberg.

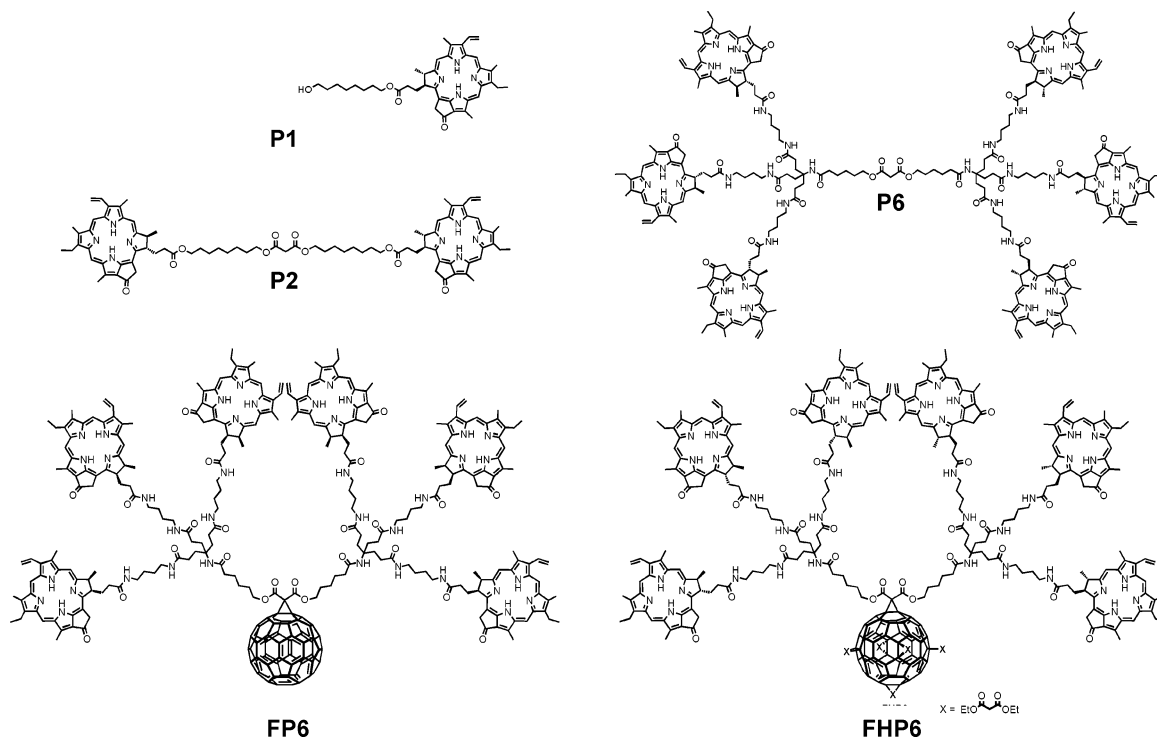


Figure 1. Structural formulas of **FHP6**, **P6**, and **FP6** and reference compounds **P1** and **P2**.

The present study is a comparative investigation of a series of three compounds, one without fullerene (**P6**) and two with an electron accepting (**FP6**) and completely substituted (**FHP6**) fullerene core, all carrying six pyropheo molecules. (See Figure 1). It is expected that the deactivation pathways of the excited states of the pyropheo chromophores are different in **P6**, **FHP6**, and **FP6** molecular systems. The influence of the fullerene core on the relative efficiency of photoinduced transfer processes is investigated in the present paper.

2. Experimental Section

2.1. Chemicals and Preparation of the Samples. Chemicals and solvents were used as received unless otherwise noted. C₆₀ was obtained from Hoechst AG/Aventis and separated from higher fullerenes by a plug filtration process.^{18,19} Pyropheophorbide *a* (pyropheo) was prepared according to literature procedures^{20,21} and its purity checked for each batch by ¹H NMR. All transformations with pyropheo were performed under a nitrogen atmosphere and with careful protection from light. Solvents were dried using standard procedures.²² Column chromatography was performed on silica gel 60 and 40–63 μm, Merck. ¹H and ¹³C NMR spectra were recorded on JEOL JMM EX 400, JEOL GX 400 and JEOL Alpha 500 instruments; an asterisk indicates a ¹H NMR resonance of the pyropheophorbide *a* moiety; the atom-indices are given according to the literature.^{23,24} FAB and EI mass spectrometry were performed with Micromass Zabspec and Varian MAT 311A machines. UV/vis spectra were recorded on a Shimadzu UV-3102 PC UV/vis NIR scanning spectrophotometer. IR spectra were taken with a Bruker Vector 22 spectrometer. The synthesis of reference compounds **P1**, **P2**, and **FP1** are described elsewhere.⁵

2.2. Absorption and Steady-State Fluorescence. The ground state absorption spectra were recorded using a commercial spectrophotometer Shimadzu UV-2501PC at room temperature. Steady-state fluorescence spectra of the investigated compounds were measured in 1 cm × 1 cm quartz optical cells using a

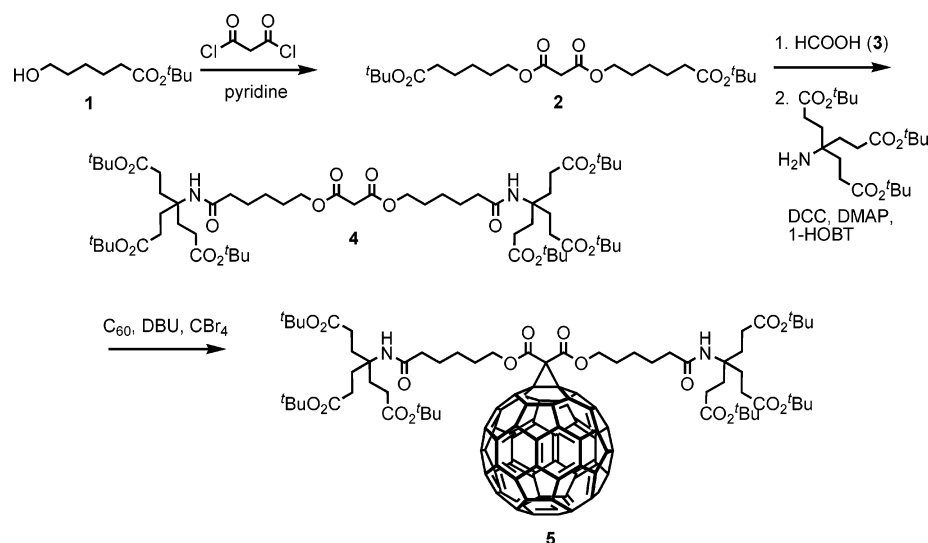
combination of a cw-Xenon lamp (XBO 150) and a monochromator (Lot-Oriel, bandwidth 10 nm) for excitation and a polychromator with a cooled CCD matrix as a detector system (Lot-Oriel, Instaspec IV).²⁵

2.3. Singlet Oxygen Generation. Photosensitized steady-state singlet oxygen luminescence was measured at 1270 nm. A cw Yb:YAG laser (Versadisk, ELS) equipped with a frequency doubling unit was used to excite the samples at 515 nm. The setup for detection of the luminescence signal has been reported previously.²⁶ To calculate the singlet oxygen quantum yield, Φ_Δ, pheophorbide *a* in DMF was used as reference (Φ_Δ = 0.52²⁶).

2.4. Time-Resolved Fluorescence Decay. Fluorescence lifetimes were measured by time-correlated single photon counting (TCSPC) technique, using the frequency doubled pulses of a Ti:Sapphire laser (Coherent Mira 900, 405 nm, FWHM 200 fs) for excitation. The instrument response function was 80 ps, as measured at excitation wavelength with Ludox. A description of the setup has been previously published.²⁷ A self-made routine was applied to minimize the least-square error between the model function convoluted with instrument response function and the measured data set.

2.5. Picosecond Transient Absorption Spectroscopy (ps-TAS). To measure transient absorption spectra, a white light continuum was generated as a test beam in a cell with D₂O/H₂O mixture using intense 25 ps single pulses from a Nd:YAG laser (PL 2143A, Ekspla) at 1064 nm. Before passing through the sample, the continuum radiation was split to get a reference spectrum. The transmitted as well as the reference beams were focused into two optical fibers and were recorded simultaneously at different traces on a CCD-matrix (Lot-Oriel, Instaspec IV). Radiation from an OPG/OPA (Ekspla PG 401/SH, tuning range 200–2300 nm) pumped by third harmonic of the same laser was used as to excite the samples at the Q_x band of the dye. The mechanical delay line allowed the measurement of the light-induced changes in the absorption spectrum at different time

SCHEME 1: Synthesis of Fullerene Precursor Compound 5



delays up to 15 ns after excitation. The optical density (OD) of all samples was 1.0 at the maximum of the last absorption Q_y band.

2.6. Molecular Modeling. In an initial step the structures of **FHP6**, **P6**, and **FP6** (See Figure 1.) were geometry optimized using the module Discover of MS Modeling. For this purpose, a COMPASS (condensed-phase optimized molecular potentials for atomistic simulation studies) force field was chosen. Minimization was performed by a combination of steepest descent, conjugate gradient, and Newton methods. In order to overcome local energy minima simulated annealing was performed afterward utilizing the Modul Forcite of MS Modeling. The molecules were heated to 700 K and then cooled to 300 K over a period of 1000 fs for 500 cycles. After each annealing step, a geometry optimization was performed applying the universal force field method. The convergence criteria for the total energy was set to 0.001 kcal/mol.²⁸

3. Results

3.1. Syntheses of P6, FP6, and FHP6. For the synthesis of **FHP6** and **FP6**, malonic acid was modified by the attachment of a C_6 -spacer unit **1** to malonyl chloride to give **2**. The *t*-butyl protecting group was removed to yield the diacid **3** (not shown) which was then coupled to a first generation Newkome-dendrimer.^{29,30} The resulting malonate **4** was coupled to C_{60} utilizing a modified Bingel-reaction leading to the important fullerene intermediate **5** (Scheme 1). ^{13}C NMR spectroscopy clearly revealed the monoadduct nature of **5** with the presence of 16 signals for the sp^2 fullerene carbon atoms (~ 145 – 139 ppm) and one for the bridgehead C atoms (72 ppm). The UV/vis absorption at 425 nm is the characteristic band for a C_{60} monoadduct. For the preparation of the reference compound **P6**, the bis-dendrimer **4** was deprotected by acidic removal of the *t*-butyl protecting groups to give the hexaacid **6** (not shown). This material was subsequently reacted with the pyropheophorbide carrier **7** under Steglich conditions to give the desired material **P6** (Scheme 2). The spectroscopic data are in accord with the given structure. In particular, the UV/vis data show the strong absorptions of the pyropheo moiety at 326, 401, 413, 510, 540, 614, and 670 nm (see Figure 2).

The synthesis of the fullerene monoadduct **FP6** with six pyropheo units attached to it utilized the abovementioned precursor **5**. After removal of the *t*-butyl protecting groups, the fullerene hexaacid **8** (not shown) was obtained quantitatively.

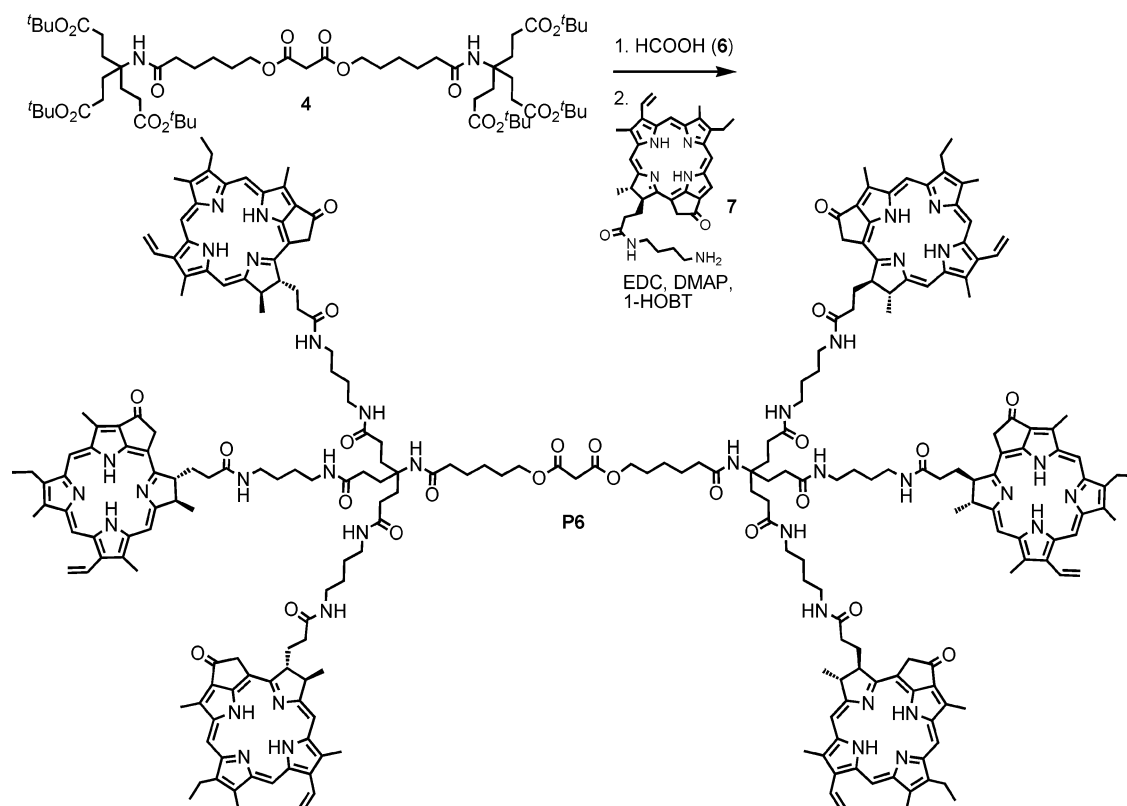
8 was immediately coupled with the pyropheophorbide system **7** which yields compound **FP6** (Scheme 3). As was observed before for multi-pyropheo systems, strong absorptions appear in the visible region of the spectra (see Figure 2).

To obtain **FHP6** five additional diethyl malonates were coupled to the fullerene core on the stage of the fullerene monoadduct **5** in good yields using template conditions. The [5:1]-hexakisadduct **9** was treated with formic acid to remove the *t*-butyl protecting groups leading to the acid **10** (not shown). Subsequent coupling with **7** gave the desired [5:1]fullerene hexakisaddukt **FHP6** (Scheme 4). Due to the attachment of five other addends, the number of ^{13}C resonances for the sp^2 carbon atoms of the fullerene cage is reduced to 12. An assignment is very difficult because of the high number of carbon resonances from the pyropheo systems. The detailed synthesis protocols can be found in the Supporting Information.

3.2. Absorption. The absorption spectra of **P6**, **FP6**, **FHP6**, and reference compounds **P1** and **P2** in DMF are shown in Figure 2. The shape of the absorption spectrum is similar to that of metal free tetrapyrroles consisting of the Soret band located at 413 nm and the splitted $Q_{x,y}$ -bands. The absorbance of **P2** containing two pyropheo units is nearly twice the absorbance of **P1** over the whole spectral range. For **P6** consisting of six pyropheo chromophores the absorbance does not increase by a factor of 6 with respect to **P1**. The $Q_y(0,0)$ absorption transition of **P1** has an extinction coefficient of $\epsilon = 4.2 \times 10^4 \text{ M}^{-1}\text{cm}^{-1}$, whereas for **P6** this value is $\epsilon = 19.2 \times 10^4 \text{ M}^{-1}\text{cm}^{-1}$. The synthesis of **FHP6** includes the addition of five malonate groups to the fullerene core resulting in broken symmetry of C_{60} .⁸ As can be seen from Figure 2, the absorbance of **FHP6** is about six times the value of **P1** over the whole UV/vis spectral region. For **FP6** the extinction coefficient of the $Q_y(0,0)$ absorption band is $\epsilon = 12.7 \times 10^4 \text{ M}^{-1}\text{cm}^{-1}$ which is lower than the value obtained for **FHP6** and even for **P6**. The fullerene core with high electron accepting capabilities in **FP6** leads to a strong decrease in absorbance of this compound, indicating the strong influence of C_{60} on the ground state properties of the attached pyropheo chromophores. The compounds **FHP6**, **FP6**, and **P6** show a pronounced splitting of the Soret band in comparison to **P1**. The $Q_y(0,0)$ band of **FHP6**, **P6**, and **FP6** is bathochromically shifted compared to **P1** by about 1, 2, and 2.5 nm, respectively.

3.3. Steady-State Fluorescence. Normalized fluorescence of the investigated compounds and the reference compound spectra

SCHEME 2: Synthesis of Reference Compound P6



are depicted in Figure 3. The fluorescence emission originates from the pyroPheo units. The fluorescence intensity of **FHP6** and **P6** is reduced compared to **P2**.

The relative fluorescence quantum yield Φ_{Frel} with respect to **P2** was measured to 33% for **FHP6** and 25% in case of **P6**. For **FP6** very weak fluorescence emission was detected. (See Table 1) The shape of the fluorescence spectra of **FHP6**, **FP6**, and **P6** is broadened compared to **P2**.

3.4. Time-Resolved Fluorescence. The fluorescence decay of **FHP6**, **P6**, and **FP6** shows a complicated character and was fitted in all cases by a four exponential functions (See Figure 4). The fluorescence decay of **FP6** exhibits a fast ($\tau_{\text{short}} = 110$ ps) and dominant quenching process of the S_1 -state. The intermediate times were determined to 0.6 and 1.7 ns, respectively. The long decay time was every time fixed to a value of $\tau_{\text{long}} = 5.7$ ns, similar to the decay time of **P2**, representing the fluorescence decay of non-interacting pyropheo chromophores.⁵ The quenching rate k_q in case of **FP6** is given by $k_q = 1/\tau_{\text{short}} - 1/\tau_{\text{long}} = 8.9 \times 10^9 \text{ s}^{-1}$. For **FHP6** and **P6**, the short component was measured to be 0.17 and 0.16 ns, respectively. The two intermediate decay components had nearly similar values (about

0.8 and 3.5 ns) for **FHP6** and **P6** compounds. It should be mentioned that all fluorescence decay times estimated for **P6** are slightly shorter compared to **FHP6**. The long decay component had the lowest amplitude (below 10%) for all three compounds under investigation.

3.5. Transient Absorption Spectroscopy. Transient absorption spectroscopy (TAS) is usually performed to follow population dynamics of different electronic states and deactivation processes after excitation. Briefly, a TAS measurement provides a set of transient absorption spectra $\Delta OD(\lambda, \Delta t)$ showing the differences in absorption before and after excitation of the sample at different delay times, Δt . Figure 5 shows the transient absorption spectra of **FHP6**, **P6**, and **FP6** at a delay time of 50 ps after excitation. For comparison, the ground state absorption spectrum and the fluorescence spectrum of **FHP6** are given at the bottom of Figure 5. A strong bleaching is observed at the S_0-S_1 transition of pyropheo around 673 nm caused by the light-induced depletion of the ground state of the molecules. Due to the small Stokes shift, the fluorescence emission of pyropheo partly superimposes the bleaching observed in the region of the S_0-S_1 transition. Between 500 and 630 nm, the light-induced excited-state absorption (S_1-S_n) of pyropheo causes an increase of the ΔOD signal whereas in the region around 480 nm the T_1-T_n induced absorption of the chromophores results in a positive ΔOD signal.³¹ The fullerene in **FHP6** and **FP6** has more than 30 times lower ground-state extinction coefficient at the excitation wavelength positioned at the Q_x band of the pyropheo molecules (515 nm), thus mainly pyropheo was excited during the TAS measurements.⁷

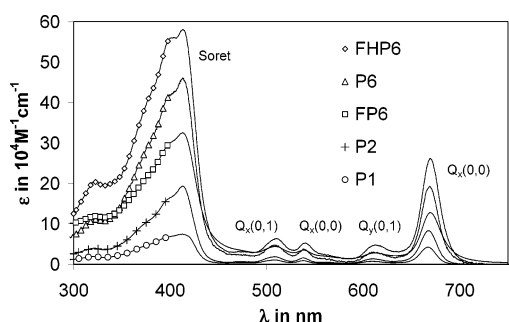
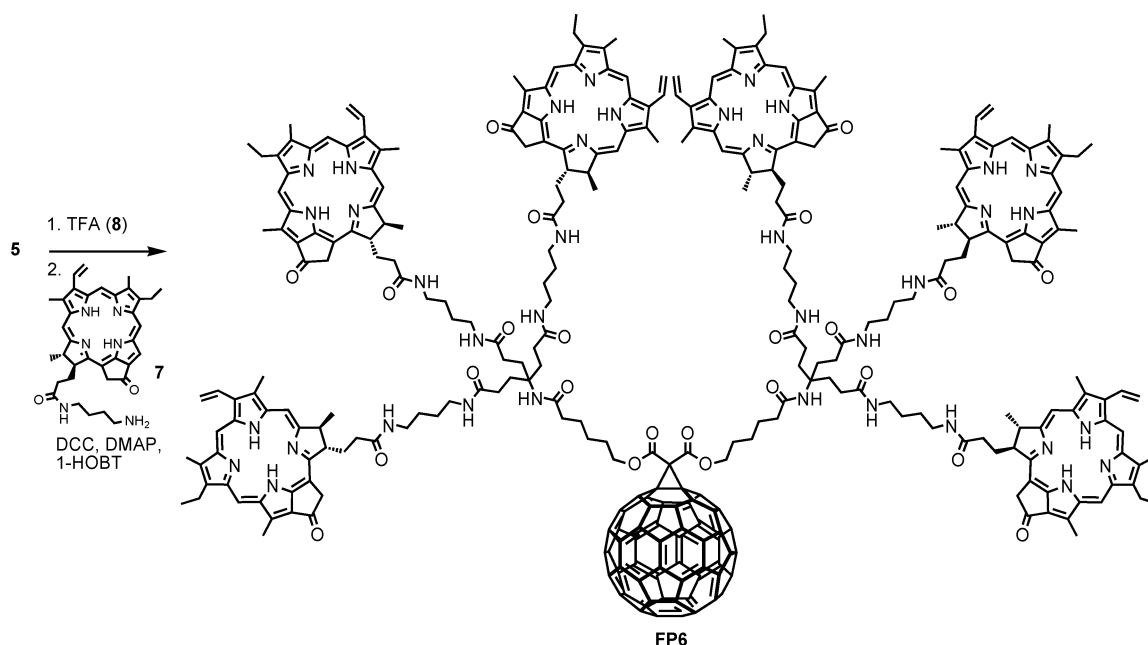
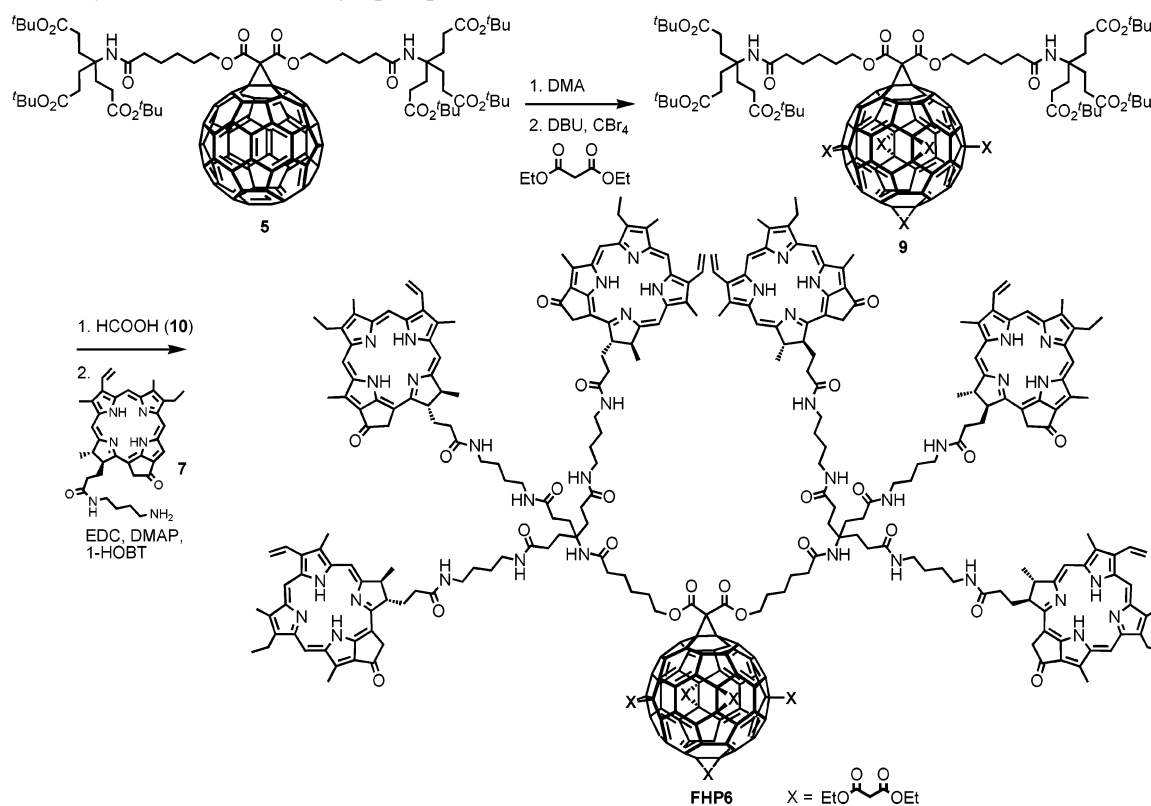


Figure 2. Absorption spectra of **FHP6**, **P6**, and **FP6** in DMF. The spectra of **P1** and **P2** are also shown for comparison.

Using the compensation method³² the change in the ground state population $\Delta S_0(t)$ and decay of the first excited singlet state population $S_1(t)$ can be determined from the ΔOD spectra in the region from 600 to 800 nm in which the S_0-S_1 transition and the fluorescence emission are partly overlapping.

SCHEME 3: Synthesis of Hexakis (Pyropheophorbide *a*)-fullerene Compound FP6**SCHEME 4: Synthesis of Hexakis (Pyropheophorbide *a*)-fullerene [5:1] Hexaadduct FHP6**

The decay of the first excited singlet state $S_1(t)$ of **FHP6**, **P6**, and **FP6** was fitted by a three exponential function. (See Figure 6) For **FHP6**, **P6**, and **FP6**, the fast decay component of the S_1 -state depopulation was measured to 49, 30, and 24 ps, respectively (see Table 1). These short times were not resolved by TCSPC setup and represent an additional process. The intermediate decay times confirm the results of TCSPC measurements. For **FP6**, the dominant deactivation process was measured to 120 ps which is in a good agreement to the value obtained from time-resolved fluorescence measurements. The long decay components measured by TAS have values of 2.8, 3.6, and 2.3 ns for **FHP6**, **P6**, and **FP6** respectively. This

component is an average value of the decay times in the nanosecond range obtained by TCSPC.

The ground state depletion of **P6**, **FHP6**, and **FP6** fitted by three exponential functions is shown in Figure 7. The short components have the same values as the fast decay times determined from transient amplification. The intermediate decay times were determined to 138, 101, 261 ps and the long decay times were fitted to 3.7, 3.1, and 5.2 ns for **FHP6**, **P6**, and **FP6**, respectively.

The intersystem crossing quantum yield (Φ_{ISC}) can be estimated by comparing the depletion of the ground state shortly after excitation ($\Delta t = 0$ ps) to the value after a long delay time

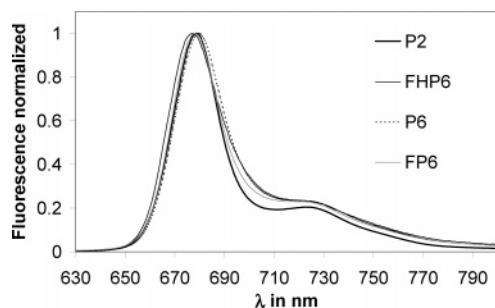


Figure 3. Fluorescence spectra of **FHP6**, **P6**, **FP6**, and reference **P2** in DMF.

TABLE 1: Selected Photophysical Parameters of FHP6, P6, and FP6 (Reference Compound P2) in DMF

sample	S ₁ decay components		Φ_{Frel}	Φ_{D}	Φ_{ISC}
	τ_{F} [ns]	amplitude			
P2	5.7		1	0.43	0.49
FHP6	0.049	0.27	0.33	0.22	0.24
	0.17	0.17			
	0.9	0.11			
	3.7	0.39			
	5.7	0.06			
P6	0.030	0.25	0.25	0.15	0.16
	0.16	0.32			
	0.7	0.09			
	3.3	0.29			
	5.7	0.05			
FP6	0.024	0.35	<0.01	0.02	0.06
	0.11	0.47			
	0.6	0.08			
	1.7	0.05			
	5.7	0.05			

($\Delta t = 15$ ns), when the population of the first excited-state is negligible.³² The intersystem crossing quantum yield of **FP6** was determined to $\Phi_{\text{ISC}} = 0.06$ which is significantly lower compared to the values for **FHP6** and **P6** (0.24 and 0.16, respectively).⁸ These different Φ_{ISC} values could be validated by singlet oxygen measurements. **FP6** has a singlet oxygen quantum yield (Φ_{Δ}) of only 0.02. For **FHP6** and **FP6**, the reduction of singlet oxygen generation compared to **P2** is not so significant, resulting in values of singlet oxygen quantum yield of 0.22 and 0.15, respectively (see Table 1).

3.6. Molecular Modeling. The structure calculations of **P6**, **FP6**, and **FHP6** were carried out in vacuo and those with the lowest potential energy were chosen for analysis (see Figure 8). All distances measured among the chromophores and C₆₀ refer to center-to-center distances. The shown possible conformations of **P6**, **FHP6**, and **FP6** have one feature in common. The pyropheo units are partly stacked together at intramolecular distances of about (9 ± 1) Å. **P6** tends to fold to a dense coil. A variety of orientations and angles between the planar pyropheo molecules could be identified. The average distance R between adjacent pyropheo units (center-to-center) in **P6** was estimated from the corresponding minimized structure to (13 ± 1) Å. The average distance between non-neighboring molecules is approximately (24 ± 2) Å. For **FP6** the situation is completely different. The molecule does not fold as dense as **P6**. The average distance of neighboring molecules is about (13 ± 3) Å but the average distance between non-neighboring units is about (32 ± 7) Å, and therefore, significantly longer compared to **P6**. It was found that one of the pyropheo units can be located in close proximity to C₆₀ at distances of around 12 Å. Such a close approach is hindered in **FHP6** because the malonate units connected to C₆₀ act as spacers.

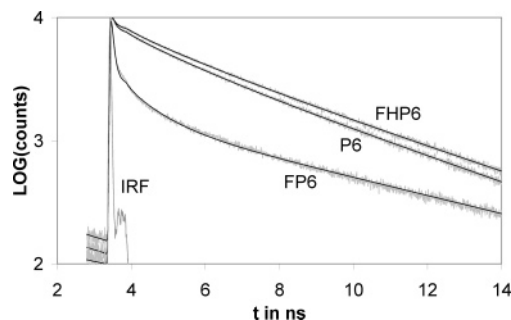


Figure 4. Time-resolved fluorescence emission decay curves of **FP6**, **P6**, and **FHP6** in DMF.

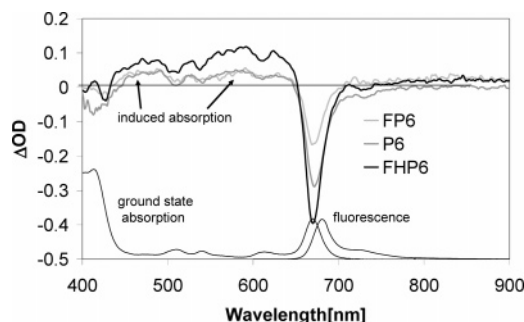


Figure 5. Transient absorption spectra of **FHP6**, **P6**, and **FP6** in DMF measured at delay time 50 ps.

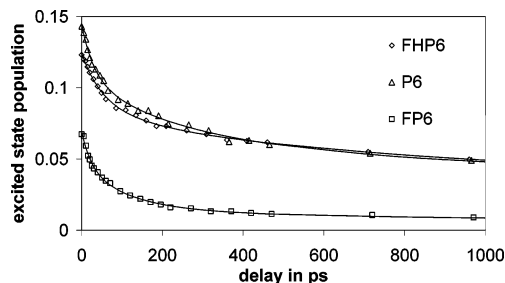


Figure 6. Excited-state population of **FHP6**, **P6**, and **FP6** as determined by ps-TAS.

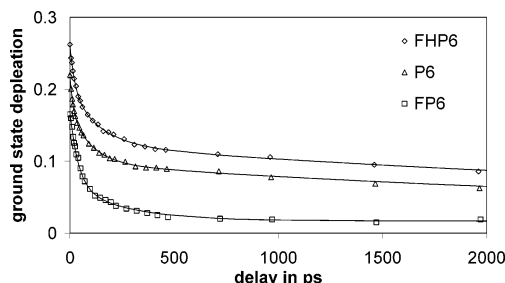


Figure 7. Ground state depletion of **FHP6**, **P6**, and **FP6** as measured by ps-TAS.

4. Discussion

Two different types of energy transfer mechanisms have been identified in **FHP6**, **P6**, and **FP6** molecules. Förster energy transfer (FET) allows the radiationless intramolecular hopping of energy from an initially excited pyropheo donor to other pyropheo units within the molecule. The other mechanism is known as excitonic interaction requiring two participating pyropheo units in a close proximity. In this case the excitation energy is delocalized over the whole dimer.^{33,34} In the first section, both types of energy transfer in **FHP6**, **P6**, and **FP6** will be discussed based on the measurements presented in the results section. Later, the focus is set on **FP6** and the possible electron transfer in this compound.

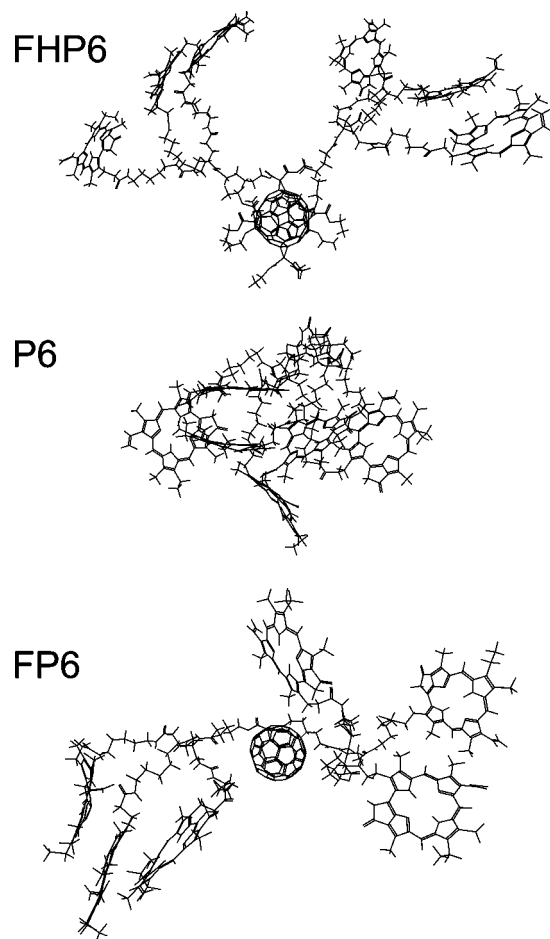


Figure 8. Energy minimized structures of **FHP6**, **P6**, and **FP6** (top to bottom) calculated with simulated annealing + geometry optimization using the modul Forcite of MS Modeling.

4.1. Energy Transfer in FHP6, P6, and FP6. FET is the result of a weak dipole–dipole interaction and requires an overlap of the emission spectrum of an energy donor (D) and the absorption spectrum of an acceptor (A). For a pyropheo–pyropheo FET a significant overlap exists, and therefore, we assume that FET may occur between adjacent pyropheo molecules. The theory developed by Förster allows estimation of energy transfer rate k_D .³⁵

$$k_D = \frac{1}{\tau_D} \left(\frac{R_0}{R_{DA}} \right)^6 \quad (1)$$

where R_{DA} is the center-to-center distance between donor and acceptor and τ_D is the lifetime of the excited pyropheo donor in the absence of any acceptor molecules. As τ_D we will use the fluorescence lifetime of **P2** in DMF measured to 5.7 ns.⁵ Förster radius R_0 can be estimated from the overlap integral of the absorption ϵ_A and normalized fluorescence spectrum I_D^n of the pyropheo molecules:³⁶

$$R_0[\text{nm}] = \sqrt[6]{\frac{8.8 \times 10^{17} \cdot k^2 \cdot \Phi_F}{n^4} \cdot \int \frac{I_D^n(\tilde{\nu}) \epsilon_A(\tilde{\nu})}{\tilde{\nu}^4} d\tilde{\nu}} \quad (2)$$

The refractive index of DMF is $n = 1.43$. The average orientation between the interacting dipole moments is not known; therefore, we assume for the orientation factor a value of $k^2 = 2/3$ corresponding to a random distribution of dipole

moments. Using these values, R_0 was calculated to 56 Å. The average distance of neighboring pyropheo units R_{DA} we assumed to be 13 Å for **P6** (see molecular modeling results). The resulting FET rate is $1.1 \times 10^{12} \text{ s}^{-1}$. This means that the excitation energy remains only one picosecond on the initially excited molecule before hopping to the nearest neighbor. Excitation jump to the more distant non-neighboring units (average $R_{DA} = 24$ Å) is more than 1 order of magnitude less probable, and the excitation should remain around 35 ps on the pyropheo moiety. For **P6**, the short component of the fluorescence lifetime was measured to 30 ps.

In the studied multichromophoric system with different distances and mutual orientations between the pyropheo units, a number of subsequent steps of FET should occur before the energy is delivered to a trap resulting in the observed average transfer time of 30 ps. As the jump to the nearest neighbor is much faster than any other process we can assume that several FET jumps take place until the energy is caught by a trap.

For **FHP6** the fast component of the fluorescence lifetime (49 ps) is longer than the value measured for **P6**. This is in agreement with molecular modeling results where the average distances between pyropheo units in **FHP6** are longer compared to **P6**. For **FP6** the fast fluorescence decay component was determined to 24 ps and this value is even shorter compared to that one of **P6**. **FP6** is not folded as dense as **P6** pointing out that a lower number of jumps occur until the dye molecules are deactivated. This may indicate the presence of another trapping process which we assume to be an electron transfer.

The absorption spectra of **FHP6**, **P6**, and **FP6** show a pronounced splitting of the Soret band. Together with the observed reduction of the fluorescence as well as ISC quantum yields compared to these values of reference **P2** compound, this is an indication for excitonic interactions between adjacent pyropheo molecules.^{34,37} The formation of pyropheo dimers in **FHP6**, **FP6**, and **P6** has two important consequences.

First the absorption cross section of a dimer is reduced in contrast to the monomer,³⁸ thus the overall absorbance should be decreased if dimer formation takes place. Indeed a significant reduced absorbance of **P6** relative to **FHP6** was observed. This is attributed to the denser folding of the **P6** molecule compared to **FHP6** (see molecular modeling results), and as a result, the probability of a trap formation is higher for **P6**. In **FHP6** the fullerene with added malonate units can be considered as a spacing unit lowering the probability of dimer formation. **FP6** demonstrated the lowest absorbance of all compounds carrying six pyropheo chromophores. As a larger spacing between the pyropheo chromophores mediated by the fullerene would lead to an increase of absorbance compared to **P6** another effect induced by C_{60} seems to be more important. The fullerene core in **FP6** with its extended π -electron system is assumed to disturb the electronic ground state properties of the attached pyropheo chromophores leading to a significant reduction of the absorbance of this compound.

Second, the pyropheo dimers can act as efficient energy traps. The arrangement of the transition dipole moments of the pyropheo units forming the dimer and the distance between them determine the properties of a trap as it was previously reported.^{12,13} The observation of an intermediate fluorescence decay time of 0.7 ns (3.3 ns) for **P6** and 0.9 ns (3.7 ns) for **FHP6** are attributed to traps with prevalent face-to-face (oblique) arrangement of the transition dipole moments.

The occurrence of the shorter fluorescence decay times (around 170 ps) one can attribute to traps with close distance between two pyropheo chromophores.

The consequence of enhanced nonradiative transitions is a reduced fluorescence intensity of **FHP6** and **P6** compared to **P2**. The fluorescence quenching of **P6** is stronger than in **FHP6**, supporting the argument that in **FHP6** dimer formation is less probable.

4.2. Electron Transfer in FP6. It was found that for **FP1** photoinduced electron transfer from initially excited pyropheo moiety to the electron accepting C₆₀-fullerene is the dominant process leading to the fast deactivation of the first excited singlet state of pyropheo with a rate of $1.8 \times 10^9 \text{ s}^{-1}$.⁴ Investigation of **FP6** revealed a strongly reduced fluorescence quantum yield, Φ_{Frel} , of 0.01 relative to **P2**, a low intersystem crossing quantum yield, Φ_{ISC} , of 0.06 and the occurrence of a fast dominant quenching process visible in the time-resolved fluorescence decay. These findings can be attributed to an efficient process deactivating the S₁ state of **FP6**. An energy transfer process to the fullerene is unfavorable because, although the first excited singlet state of C₆₀ (1.75 eV)³⁹ is energetically close to the singlet state of pyropheo (1.84 eV), the extinction coefficient of C₆₀ monoadduct in the region of the fluorescence band of pyropheo is very low, thus the overlap integral and the Förster radius are very small too.⁴⁰ For **FHP6** the reduction of fluorescence (quantum yield 0.33 relative to **P2**) and intersystem crossing quantum yield ($\Phi_{\text{ISC}} = 0.24$) is not as strong as for **FP6**. As the first electron reduction potential of fullerene hexakisadduct is relatively high, about 0.8 V lower than for the fullerene monoadduct,⁴¹ the electron accepting capabilities of the fullerene moiety in **FHP6** are strongly reduced compared to **FP6**.

From a thermodynamic point of view the question of a possible electron transfer for **FP6** between excited pyropheo donor (D) and C₆₀ acceptor (A) can be addressed by calculating the free energy change using the Rehm–Weller equation:^{42–44}

$$\Delta G^0 = e[E_{1/2}^{\text{ox}}(\text{D/D}^+) - E_{1/2}^{\text{red}}(\text{A/A}^-)] - \Delta E^* - \frac{e^2}{4\pi\epsilon_0\epsilon_s R} - \frac{e^2}{8\pi\epsilon_0} \left[\frac{1}{r_{d+}} + \frac{1}{r_{a-}} \right] \left[\frac{1}{\epsilon_{\text{ref}}} - \frac{1}{\epsilon_s} \right] \quad (3)$$

The half-wave oxidation potential of the pyropheo in DMF is $E_{1/2}^{\text{ox}}(\text{D/D}^+) = 0.42 \text{ V}$.⁴⁵ The first step half-wave reduction potential of a similar fullerene monoadduct (C₆₀H₂) dissolved in PhCN was reported to be -1.05 V (vs Fc⁺/Fc).⁴⁶ By referencing this value to the SCE electrode (+0.40 V)⁴⁷ and applying a solvent correction (+0.02 V for PhCN → DMF), we assume a reduction potential of $E_{1/2}^{\text{red}}(\text{A/A}^-) = -0.63 \text{ V}$ for the C₆₀ monoadduct in DMF. ΔE^* is the energy difference between first excited singlet and ground states of pyropheo which was derived from the absorption and fluorescence spectra to $\Delta E^* = 1.84 \text{ eV}$. The effective radii of the fullerene anion is $r_{a-} = 4 \text{ Å}$,⁴⁸ whereas the value of the pyropheo donor cation is $r_{d+} = 4.4 \text{ Å}$. The separation distance between donor and acceptor was assumed to be $R = 12 \text{ Å}$. The last two values were estimated from molecular modeling simulation. The dielectric constant of DMF is $\epsilon_s = \epsilon_{\text{ref}} = 37$. For the free energy change we calculated a value of $\Delta G^0 = -0.82 \text{ eV}$. A negative ΔG^0 implies that the electron transfer from photoexcited pyropheo to the fullerene core is an exergonic reaction. The energy of the charge separated state is $E_{\text{CS}} = \Delta E^* + \Delta G^0 = 1.02 \text{ eV}$. This value lies below the energy of the first excited singlet as well as triplet state of pyropheo. When donor and acceptor are spaced by more than $\sim 5 \text{ Å}$, electron transfer can be treated in the nonadiabatic or weak coupling limit.⁴⁹ The widely used expression developed by

Marcus⁵⁰ allows the calculation of the transfer rate k_{ET} :

$$k_{\text{ET}} = \left(\frac{4\pi^3}{h^2 \lambda k_{\text{B}} T} \right)^{1/2} V^2 \exp \left[- \frac{(\Delta G^0 + \lambda)^2}{4\lambda k_{\text{B}} T} \right] \quad (4)$$

In the first term h is the Planck constant, $T = 293 \text{ K}$ is the room temperature, k_{B} is the Boltzmann constant, and λ is the reorganization energy, λ is the sum of the intramolecular reorganization energy λ_{I} and the solvent reorganization energy λ_{S} . The intramolecular reorganization energy is around 0.3 eV,^{51,52} whereas λ_{S} can be approximated by

$$\lambda_{\text{S}} = \frac{e^2}{4\pi\epsilon_0} \left[\frac{1}{n^2} - \frac{1}{\epsilon_s} \right] \left[\frac{1}{2r_{a-}} + \frac{1}{2r_{d+}} - \frac{1}{R} \right] \quad (5)$$

Using the values already mentioned, the solvent reorganization energy is $\lambda_{\text{S}} = 1.08 \text{ eV}$. The total reorganization energy is then calculated to $\lambda = 1.38 \text{ eV}$.

In order to estimate the electron-transfer rate, the coupling matrix element V is also needed. A precise determination would require a quantum mechanical approach, but it was shown that V^2 can be approximated by the following term:⁵³

$$V^2 = V_0^2 \exp(-\beta(R - r_{a-} - r_{d+})) \quad (6)$$

The highly flexible spatial arrangement of the pyropheo donor and C₆₀ acceptor may allow conformations, in which the through-space distance is lower than the through-bond pathway. For this reason electron transfer may also occur by a through-space mechanism, even if the coupling matrix element at contact (V_0) is usually smaller than for a through-bond situation.^{54,55} For fullerene-based donor acceptor systems, high values of $V_0 = 100 \text{ cm}^{-1}$ for through-bond ET have been reported which we will be used as an upper limit for the molecular systems investigated. The distance attenuation factor β for saturated hydrocarbon spacers typically exhibit values of 1 Å^{-1} .^{56,57} Similar factors have been obtained for pure liquid electron transfer in polar solvents; therefore, the damping factor is assumed to be $\beta = 1 \text{ Å}^{-1}$, approximating both through-bond and through space ET.^{58,59}

Using the values mentioned above, the electron-transfer rate was calculated to $k_{\text{ET}} = 8.9 \times 10^9 \text{ s}^{-1}$ or $\tau_{\text{ET}} = 112 \text{ ps}$. The determined quenching rate from the observed short fluorescence decay component (110 ps) of **FP6** is $k_{\text{q}} = 8.9 \times 10^9 \text{ s}^{-1}$ (see section 3.3), which is in very good agreement with this theoretical value. Comparable electron-transfer rates have been reported for self-assembled zinc porphyrin-fulleropyrrolidine dyads in which donor and acceptor are spaced by about 10 Å .⁶⁰

After photoexcitation of the **FP6** molecule, an intramolecular competition between energy delivery to the traps and transport to the pyropheo chromophore located close to the fullerene takes place. On the one hand, the energy transfer to traps reduces the probability of an electron transfer. On the other hand, FET facilitates delivery of excitation from the periphery of the system to the pyropheo chromophore in close distance with the fullerene. As result, the probability of electron transfer is increased and, therefore, becomes the major deactivation pathway in the **FP6** molecule.

5. Conclusions

The flexibility of the dendron system connecting the six pyropheophorbide *a* molecules among one another (**P6**) and coupling it to a fullerene core (**FHP6**, **FP6**) allows a huge

variety of possible conformations. In such systems with high degrees of freedom, complex interactions are conceivable.

Excitonic interactions between adjacent pyropheo units were observed in **FHP6**, **P6**, and **FP6** leading to the formation of efficient energy traps. The excitation energy can hop from an initially excited pyropheo unit by Förster energy transfer to every other pyropheo molecule. Because the Förster transfer rate decreases with $1/r^6$, the jump to the nearest neighbor (distance 13 Å for **P6**) is much more probable than to non-neighboring pyropheos (average distance 24 Å for **P6**, 32 Å for **FP6**, and 38 Å for **FHP6**). For **P6** and **FHP6**, a cascade of energy transfers is likely to occur until the energy vanishes in the dimer trap. Also, but with minor probability, the dye molecules may be deactivated via fluorescence or intersystem crossing to the first excited triplet state of pyropheo.

In **FP6**, molecular simulation showed that one pyropheo unit can be located in closer proximity to the electron-accepting C₆₀ fullerene core. This opens up the possibility of a fast electron transfer from photoexcited pyropheo unit to the fullerene core. Our measurements suggest that such a fast ET is indeed the main deactivation pathway. The **FP6** molecular system can be considered as a combination of a light-harvesting system consisting of several separate pyropheo molecules and a charge-separating center. The formation of intramolecular sub divisions with different functions in a spontaneous self-assembling way may give ideas for the design of artificial molecular complexes of photosynthesis.

Acknowledgment. We thank the DFG (E.A.E., B.R.: grant no. RO 1042/9-4; E.A.E., B.R., M.M.: grant no. RO 1042/11-1; A.H., M.H., N.J.: grant no. HI 468/11-1). We also thank Mrs. Gisela Wöhlecke (Berlin) for technical assistance and Priv.-Doz. Dr. Andreas Humeny (Erlangen) for performing the MALDI-TOF experiments.

Supporting Information Available: Synthesis protocols for compound 2–6, **7a**, **8–10**, **FP6**, **FHP6**; This material is available free of charge via the Internet at <http://pubs.acs.org>.

References and Notes

- Wiehe, A.; Senge, M. O.; Schäfer, A.; Speck, M.; Tannert, S.; Kurreck, H.; Röder, B. *Tetrahedron* **2001**, *57*, 10089.
- Palacios, R. E.; Kodis, G.; Gould, S. L.; de la Garza, L.; Brune, A.; Gust, D.; Moore, T. A.; Moore, A. L. *ChemPhysChem* **2005**, *6*, 2359.
- Imahori, H.; Fukuzumi, S. *Adv. Funct. Mater.* **2004**, *14*, 525.
- Ermilov, E. A.; Al-Omari, S.; Helmreich, M.; Jux, N.; Hirsch, A.; Röder, B. *Opt. Commun.* **2004**, *234*, 245.
- Ermilov, E. A.; Al-Omari, S.; Helmreich, M.; Jux, N.; Hirsch, A.; Röder, B. *Chem. Phys.* **2004**, *301*, 27.
- Helmreich, M.; Ermilov, E. A.; Meyer, M.; Jux, N.; Hirsch, A.; Röder, B. *J. Am. Chem. Soc.* **2005**, *127*, 8376.
- Omari, S.; Ermilov, E. A.; Helmreich, M.; Jux, N.; Hirsch, A.; Röder, B. *Appl. Phys. B* **2004**, *79*, 617.
- Ermilov, E. A.; Hackbarth, S.; Al-Omari, S.; Helmreich, M.; Jux, N.; Hirsch, A.; Röder, B. *Opt. Commun.* **2005**, *250*, 95.
- D'Souza, F.; Ito, O. *Coord. Chem. Rev.* **2005**, *249*, 1410.
- Segura, J.; Giacalone, F.; Gómez, R.; Martín, N.; Guldí, D.; Luo, C.; Swartz, A.; Riedel, I.; Chirvase, D.; Parisi, J.; Dyakonov, V.; Sariciftci, N. S.; Pädinger, F. *Mater. Sci. Eng. C* **2005**, *25*, 835.
- Konishi, T.; Ikeda, A.; Shinkai, S. *Tetrahedron* **2005**, *61*, 4881.
- Hackbarth, S.; Ermilov, E. A.; Röder, B. *Opt. Commun.* **2005**, *248*, 295.
- Röder, B.; Ermilov, E. A.; Hackbarth, S.; Helmreich, M.; Jux, N. *SPIE* **2006**, *6192*, 495.
- Dichtel, W. R.; Hecht, S.; Fréchet, J. M. J. *Org. Lett.* **2005**, *7*, 4451.
- Röder, B. in *Encyclopedia Analytical Chemistry*; Meyers, R.A., Ed.; Wiley: Chichester, 2000, 302.
- Rancan, F.; Helmreich, M.; Mölich, A.; Jux, N.; Hirsch, A.; Röder, B.; Witt, C.; Böhm, F. *J. Photochem. Photobiol. B* **2005**, *80*, 1.
- Paul, A.; Hackbarth, S.; Mölich, A.; Luban, C.; Oelckers, S.; Böhm, F.; Röder, B. *Laser Phys.* **2003**, *13*, 22.
- Reuther, U. Ph.D. Dissertation, University of Erlangen-Nürnberg, 2001.
- Isaacs, L.; Wehrsig, A.; Diederich, F. *Helv. Chim. Acta* **1993**, *76*, 1231.
- Risch, N.; Reich, H.; Schormann, A.; Brockmann, H. *Liebigs Ann. Chem.* **1981**, 1519.
- Wasielowski, M. R.; Svec, W. A. *J. Org. Chem.* **1980**, *45*, 1969.
- Perrin, D. D.; Amarego, W. L. F. *Purification of Laboratory Chemicals*, 3rd ed.; Pergamon Press: Oxford, 1988.
- G. L. Closs, J. J. Katz, F. C. Pennington, M. R. Thomas, H. H. Strain *J. Am. Chem. Soc.* **1963**, *85*, 3809.
- Smith, K. M.; Unsworth, J. F. *Tetrahedron* **1975**, *31*, 367.
- Korth, O.; Hanke, T.; Rückmann, I.; Röder, B. *Exp. Technol. Phys.* **1995**, *41*, 25.
- Spiller, W.; Kliesch, H.; Wöhrle, D.; Hackbarth, S.; Röder, B.; Schnurpfeil, G. *J. Porphyrins Phthalocyanines* **1998**, *2*, 145.
- Makarov, S.; Litwinski, C.; Ermilov, E. A.; Suvorova, O.; Röder, B.; Wöhrle, D. *Chem. Eur. J.* **2006**, *12*, 1468.
- Material Studio, Packages: Discover and Forcite, Version 3.2, Accelrys, Inc: San Diego.
- Newkome, G. R.; Behera, R. K.; Moorefield, C. N.; Baker, G. R. *J. Org. Chem.* **1991**, *56*, 7162.
- Newkome, G. R.; Nayak, A.; Behera, R. K.; Moorefield, C. N.; Baker, G. R. *J. Org. Chem.* **1991**, *57*, 358.
- Zeug, A.; Rückmann, I.; Röder, B. *J. Opt. B* **2001**, *3*, S251.
- Rückmann, I.; Zeug, A.; Herter, R.; Röder, B. *J. Photochem. Photobiol.* **1997**, *66*, 576.
- Helenius, V.; Monshouwer, R.; van Grondelle, R. *J. Phys. Chem. B* **1997**, *101*, 10554.
- Kasha, M.; Rawls, H. R.; Ashraf El-Bayoumi, M. *Pure Appl. Chem.* **1965**, *11*, 371.
- Förster, T. *Ann. Phys.* **1948**, *2*, 55.
- Kleima, F. J.; Hofmann, E.; Gobets, B.; van Stokkum, I. H. M.; van Grondelle, R.; Diederichs, K.; van Amerongen, H. *Biophys. J.* **2000**, *78*, 344.
- Kasha, M. *Discuss. Faraday Soc.* **1950**, *9*, 14.
- Eichwurz, I.; Stiel, H.; Röder, B. *J. Photochem. Photobiol. B* **2000**, *54*, 194.
- van Hal, P. A.; Knol, J.; Langeveld-Voss, B. M. W.; Meskers, S. C. J.; Hummelen, J. C.; Janssen, R. A. J. *J. Phys. Chem.* **2000**, *104*, 5974.
- Sun, Y.-P.; Guduru, R.; Lawson, G. E.; Mullins, J. E.; Guo, Z.; Quinlan, J.; Bunker, C. E.; Gord, J. R. *J. Phys. Chem. B* **2000**, *104*, 4625.
- Boudon, C.; Gisselbrecht, J.-P.; Gross, M.; Isaacs, L.; Anderson, H. L.; Faust, R.; Diederich, F. *Helv. Chim. Acta* **1995**, *78*, 1334.
- Petersson, K.; Wiberg, J.; Ljungdahl, T.; Mårtensson, J.; Albinsson, B. *J. Phys. Chem. A* **2006**, *110*, 319.
- Rehm, D.; Weller, A. *Ber. Bunsenges. Phys. Chem.* **1969**, *73*, 834.
- Rehm, D.; Weller, A. *Isr. J. Chem.* **1970**, *8*, 259.
- Osuka, A.; Wada, Y.; Shinoda, S. *Tetrahedron* **1996**, *52*, 4311.
- Guarr, T. F.; Meier, M. S.; Vance, V. K.; Clayton, M. *J. Am. Chem. Soc.* **1993**, *115*, 9862.
- Gagne, R. R.; Koval, C. A.; Lisensky, G. C. *Inorg. Chem.* **1980**, *19*, 2854.
- Chibisov, A. *Russ. Chem. Rev.* **1981**, *50*, 615.
- Venturoli, G.; Drepper, F.; Williams, J. C.; Allen, J. P.; Lin, X.; Mathis, P. *Biophys. J.* **1998**, *74*, 3226.
- Marcus, R.; Sutin, N. *Biochim. Biophys. Acta* **1985**, *811*, 265.
- Gould, I. R.; Ege, D.; Moser, J. E.; Farid, S. *J. Am. Chem. Soc.* **1990**, *112*, 4290.
- Gould, I. R.; Young, R. H.; Moody, R. E.; Farid, S. *J. Phys. Chem.* **1991**, *95*, 2068.
- De, A. K.; Sinha, S.; Nandy, S. K.; Ganguly, T. *J. Chem. Soc. Faraday Trans.* **1998**, *94*, 1695.
- Sakata, Y.; Imahori, H.; Tsue, H.; Higashida, S.; Akiyama, T.; Yoshizawa, E.; Aoki, M.; Yamada, K.; Hagiwara, K.; Taniguchi, S.; Okada, T. *Pure Appl. Chem.* **1997**, *69*, 1951.
- Weiss, E. A.; Stinks, L. E.; Lukas, A. S.; Chernick, E. T.; Ratner, M. A.; Wasielewski, M. R. *J. Phys. Chem. B* **2004**, *108*, 10309.
- Murata, S.; Nishimura, M.; Matsuzaki, S. Y.; Tachiya, M. *Chem. Phys. Lett.* **1994**, *219*, 200.
- Gray, H. B.; Winkler, J. R. *PNAS* **2005**, *102*, 3534.
- Tavernier, H. L.; Kalashnikov, M. M.; Fayer, M. D. *J. Chem. Phys.* **2000**, *113*, 10191.
- Saik, V. O.; Goun, A. A.; Nanda, J.; Shirota, K.; Tavernier, H. L.; Fayer, M. D. *J. Phys. Chem. A* **2004**, *108*, 6696.
- D'Souza, F.; Deviprasad, G. R.; Zandler, M. E.; Hoang, V. T.; Klykov, A.; VanStipdonk, M.; Perera, A.; El-Khouly, M. E.; Fujitsuka, M.; Ito, O. *J. Phys. Chem. A* **2002**, *106*, 3243.